Bull. Mater. Sci., Vol. 39, No. 3, June 2016, pp. 737–742. © Indian Academy of Sciences.
DOI 10.1007/s12034-016-1198-7

Effects of Nb doping on the microstructure, ferroelectric and piezoelectric properties of $0.7BiFeO_3$–$0.3BaTiO_3$ lead-free ceramics

XIAOLAN WU, LINGLING LUO, NA JIANG, XIAOCHUN WU* and QIAOJI ZHENG
College of Chemistry and Materials Science, Sichuan Normal University, Chengdu 610066, China

MS received 3 November 2014; accepted 1 December 2015

Abstract. **Donor-doped lead-free $Bi_{0.7}Ba_{0.3}(Fe_{0.7}Ti_{0.3})_{1-x}Nb_{0.66x}O_3$ + 1 mol% MnO_2 ceramics were prepared by a conventional oxide-mixed method and the effects of Nb-doping on microstructure, piezoelectric and ferroelectric properties of the ceramics were investigated. All the ceramics exhibit a pure perovskite structure with rhombohedral symmetry. The grain growth of the ceramics is inhibited after the addition of Nb doping. High electric insulation ($R = 10^9$–10^{10} Ω·cm) and the poor piezoelectric performance and weak ferroelectricity are observed after the addition of Nb_2O_5 in the ceramics. Different from the donor effect of Pb-based perovskite ceramics, the introduction of Nb into $0.7BiFeO_3$–$0.3BaTiO_3$ degrades the piezoelectricity and ferroelectricity of the ceramics. The $Bi_{0.7}Ba_{0.3}(Fe_{0.7}Ti_{0.3})_{1-x}Nb_{0.66x}O_3$ + 1 mol% MnO_2 ceramic with $x = 0$ exhibits the optimum piezoelectric properties with $d_{33} = 133$ pN C^{-1} and $k_p = 0.29$ and high Curie temperature ($T_C = 603$°C).**

Keywords. **Lead-free ceramics; $BiFeO_3$–$BaTiO_3$; ferroelectric properties; piezoelectric properties.**

1. Introduction

Lead-based piezoelectric ceramics with a perovskite structure, represented by $Pb(Zr,TiO_3)$ (PZT) and PZT-based multi-system, have been widely used in transformers, sensors, actuators and other electromechanical devices due to their high piezoelectric response. However, the use of these lead-based ceramics has caused serious environmental problems because of the strong toxicity of lead oxide and its high vapour pressure during sintering process. Therefore, lead-free ceramics have attracted considerable attention in recent years.

As a classic single-phase multiferroic material, $BiFeO_3$ (BFO) has attracted much attention due to its coexistence of ferroelectricity and ferromagnetism [1]. It has a rhombohedrally distorted pervoskite structure of $R3c$ space group and possesses high ferroelectric Curie temperature (T_C) of ~830°C and an antiferromagnet Néel temperature (T_N) of ~370°C [2]. Therefore, $BiFeO_3$ material may have potential applications in various advanced devices [1,3]. However, it is well known that pure $BiFeO_3$ ceramic has a large electric leakage due to the reduction of Fe ions from Fe^{3+} to Fe^{2+} during the sintering process [4]. In addition, low resistivity usually causes lower magnetoelectric effect [3,5]. The semiconducting property of $BiFeO_3$ ceramic leads to high dielectric loss and poorly saturated ferroelectric hysteresis loops. Moreover, single-phase BFO with pure perovskite structure is difficult to synthesize due to the narrow temperature range of phase stabilization, and thus some impurity phases (e.g., $Bi_2Fe_4O_9$, $Bi_{25}FeO_{40}$, etc.) are usually detected [1,4,6]. Hence, to enhance electric insulation and inhibit the formation of impurity phase of BFO, some effective methods such as A-site or B-site ions substituted by other ions (e.g., La^{3+}, Mn^{4+}, Ni^{2+}, etc.) [7–9] and form solid solution of $BiFeO_3$ with other ABO_3 perovskite structure materials (e.g., $BaTiO_3$ and $Bi_{0.5}K_{0.5}TiO_3$, etc.) have been developed [4,10]. Among these BFO-based materials, $BiFeO_3$–$BaTiO_3$ (BFO–BT) ceramic is considered as one of the most promising multiferroic systems [11,12]. From previous studies, Mn-modified BFO–BT ceramics show good piezoelectricity and temperature stability [13–15]. On the other hand, it is well known that donor doping is an important approach to enhance the piezoelectric properties of perovskite piezoelectric ceramics. Among donor ions, Nb^{5+} is most frequently used to improve the piezoelectricity of piezoelectric materials as a donor aid. For instance, the piezoelectric property of pure PZT ($d_{33} \sim 240$ pC N^{-1}) is increased significantly after the doping of Nb ($d_{33} \sim 385$–640 pC N^{-1}) [16–19]. However, to our knowledge, there is no report on the effect of Nb doping on the piezoelectric and ferroelectric properties of BFO–BT ceramics. Therefore, in this work, Nb-doped $BiFeO_3$–$BaTiO_3$ ceramics, $Bi_{0.7}Ba_{0.3}(Fe_{0.7}Ti_{0.3})_{1-x}Nb_{0.66x}O_3$ + 1 mol% MnO_2 ($x = 0$, 0.0025, 0.05, 0.075, 0.01, 0.0125, 0.015, 0.0175 and 0.02), were prepared by the solid-state reaction method and the phase structure, piezoelectric and ferroelectric properties of the ceramics were investigated.

*Author for correspondence (wuxiaochun@sicnu.edu.cn)

2. Experimental

Ceramics of $Bi_{0.7}Ba_{0.3}(Fe_{0.7}Ti_{0.3})_{1-x}Nb_{0.66x}O_3$ + 1 mol% MnO_2 with $x = 0$, 0.0025, 0.05, 0.075, 0.01, 0.0125, 0.015, 0.0175 and 0.02 were fabricated in air by the conventional solid-state reaction. Stoichiometric amounts of Bi_2O_3 (99%), Fe_2O_3 (99%), $BaCO_3$ (99%), TiO_2 (98.5%) were weighed and calcined at 800°C for 4 h in a crucible. Subsequently, the target amount of Nb_2O_5 (99.99%) and MnO_2 (99.9%) additives were added after the calcination. The powders were pressed into pellets and sintered at 960°C for 2 h. Both surfaces of the sintered ceramics fired silver electrodes at 650°C for 30 min. The samples were pooled at 100–120°C for 30 min and then cooled to room temperature in a silicone oil bath under a d.c. field of 5 kV mm^{-1}.

The crystal structure was determined by use of an X-ray diffractometer with CuKα ($\lambda = 1.540598$ Å) radiation (Smart Lab; Rigaku, Tokyo, Japan), 0.01° scan step and continuous scanning type in the 2θ range of 20–70°. The lattice parameters of the ceramics were refined by the Rietveld refinement using a general diffraction/reflectivity analysis programme MAUD [20]. The microstructure of the samples was examined by scanning electron microscopy (SEM, FEI-Quanta 250). The relative dielectric constant ε_r and loss tangent tan δ at 1 MHz were measured as a function of temperature using an LCR meter (Agilent E4980A) and temperature controlled probe stage (Linkam TS1500E). The polarization–electric field (P–E) loops at room temperature were determined using a ferroelectric tester (Premier II, Radiant Technologies Inc.). The piezoelectric constant d_{33} was measured using a piezo-d_{33} meter (ZJ-6A, China). The planar mode electromechanical coupling coefficient k_P was measured by the resonance method according to the IEEE Standards 176 using an impedance analyzer (Agilent 4294A).

3. Results and discussion

Figure 1 shows the room temperature XRD patterns of $Bi_{0.7}Ba_{0.3}(Fe_{0.7}Ti_{0.3})_{1-x}Nb_{0.66x}O_3$ ceramics. All ceramics exhibit pure perovskite phase and no second phases could be detected. As well known, the radius of Nb^{5+} (0.69 Å) is close to that of Ti^{4+} (0.60 Å) and Fe^{3+} (0.64 Å). Therefore, Nb^{5+} ions most likely enter the B sites and substitutes for Ti^{4+} or Fe^{3+}, serving as donor-type dopant. The ceramic with $x = 0$ exhibits rhombohedrally distorted structure, which is in accordance with previous reports of the BFO–BT-x system with $x < 33$ mol% [21]. A general diffraction/reflectivity analysis programme MAUD was used to perform a full-pattern matching using the Rietveld method and refine the cell parameters. According to the rhombohedral structure ($R3c$), the compositional dependences of the lattice parameters (a, c and V) and fitting parameters (R_{wp} and S) of the BFO–BT–Nb-x ceramics are shown in table 1. From table 1, for all the refinements, the values of the reliability R_{wp} of 9.81–13.88% (<15%) and the goodness-of-fit indicator S of 1.27–1.83 (<2) are obtained, suggesting a good matching between the observed and calculated patterns. Diffraction peaks of all the ceramics can be indexed and refined to the rhombohedral structure $R3c$ by the Rietveld method. The observed lattice parameters a, c and V remain the slight fluctuations of 5.6478–5.6511 Å^3/13.8207–13.8399 Å^3/382.0930–382.5182 Å^3. From figure 1b, diffraction angle has a slight shift to lower diffraction angel, indicating that the lattice distortion of the ceramics was dependent on the doping amount of Nb_2O_5.

Figure 2 shows the SEM graphs of the surface microstructure of the $Bi_{0.7}Ba_{0.3}(Fe_{0.7}Ti_{0.3})_{1-x}Nb_{0.66x}O_3$ ceramics with $x = 0$–0.02. From figure 2a, the ceramic without doping (i.e., $x = 0$) is well-crystallized with an average grain size

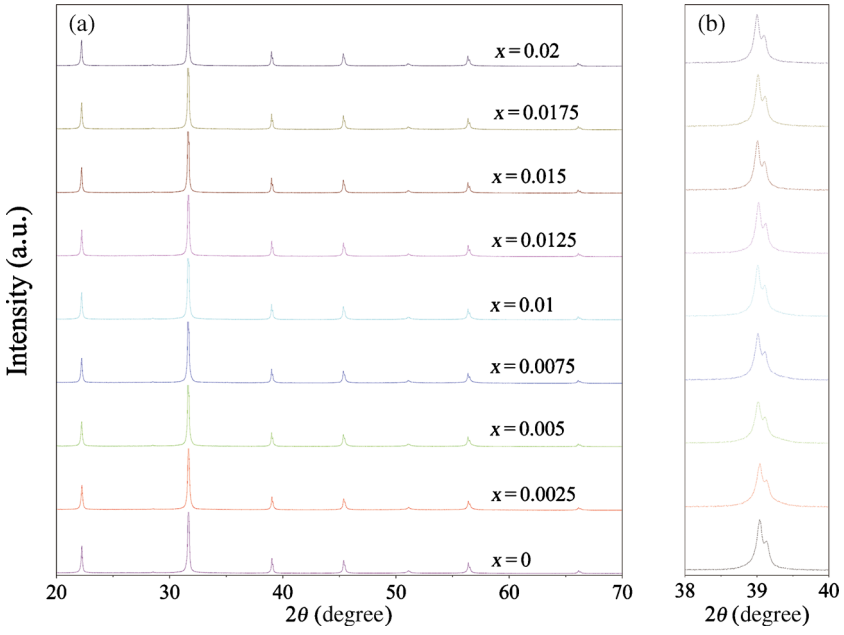

Figure 1. X-ray diffraction patterns of the $Bi_{0.7}Ba_{0.3}(Fe_{0.7}Ti_{0.3})_{1-x}Nb_{0.66x}O_3$ ceramics.

Table 1. Lattice parameters (a, c and V) and fitting parameters (R_{wp} and S) of the BFO–BTO–Nb−x ceramics.

	Lattice parameters			R factor (%)	
x	a (Å)	c (Å)	V (Å^3)	R_{wp}	S
0	5.6479(5)	13.8354(3)	382.2125(8)	12.95	1.65
0.0025	5.6501(1)	13.8207(3)	382.0985(8)	13.01	1.72
0.005	5.6506(6)	13.8284(2)	382.3856(2)	9.81	1.27
0.0075	5.6511(1)	13.8310(1)	382.5181(5)	10.57	1.37
0.01	5.6506(8)	13.8307(6)	382.4530(3)	12.83	1.69
0.0125	5.6506(1)	13.8291(8)	382.3998(6)	13.70	1.75
0.015	5.6501(8)	13.8398(4)	382.4782(1)	13.52	1.71
0.075	5.6490(1)	13.8398(5)	382.0930(0)	13.69	1.74
0.02	5.6478(4)	13.8316(4)	382.1943(0)	13.88	1.83

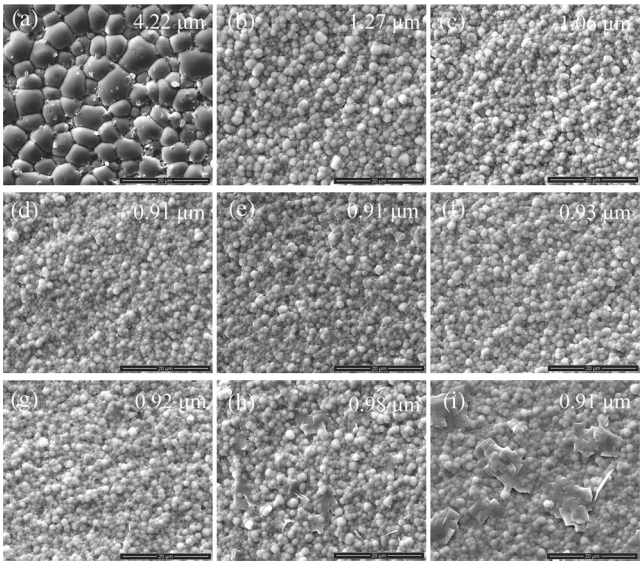

Figure 2. SEM graphs of the surface microstructure of the $Bi_{0.7}Ba_{0.3}(Fe_{0.7}Ti_{0.3})_{1-x}Nb_{0.66x}O_3$ ceramics with (**a**) $x = 0$, (**b**) 0.0025, (**c**) 0.005, (**d**) 0.0075, (**e**) 0.01, (**f**) 0.0125, (**g**) 0.015, (**h**) 0.0175 and (**i**) 0.02.

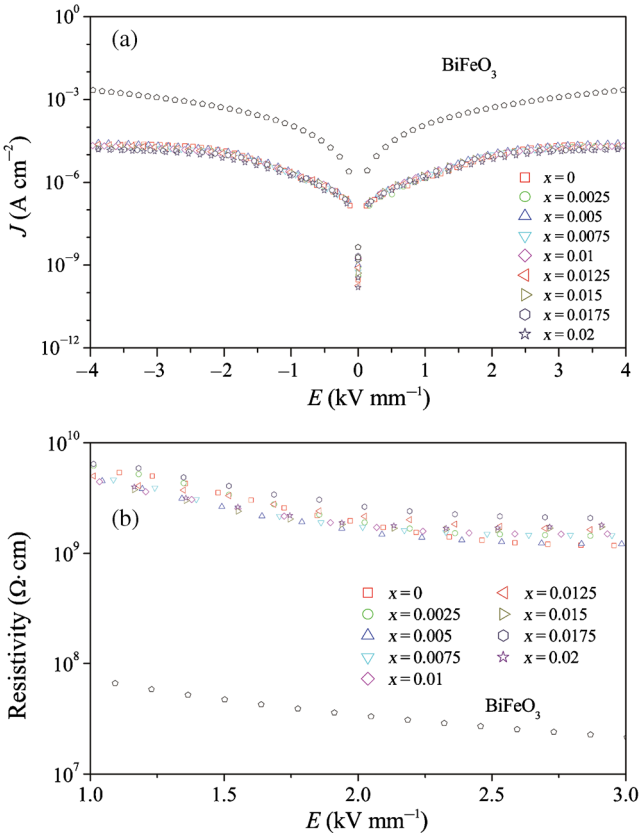

Figure 3. (**a**) Leakage current density J of the $Bi_{0.7}Ba_{0.3}(Fe_{0.7}Ti_{0.3})_{1-x}Nb_{0.66x}O_3$ ceramics and the pure BFO sintered at 775°C for 2 h as a function of the electric field and (**b**) dependences of resistivity R of the $Bi_{0.7}Ba_{0.3}(Fe_{0.7}Ti_{0.3})_{1-x}Nb_{0.66x}O_3$ and pure BFO ceramics on the electric field E.

D_A of 4.22 μm and have clear grain boundaries. However, the grain sizes decrease significantly to 0.91 μm with x increasing to 0.02, indicating that the doping of Nb inhibits the grain growth of the ceramics, which may be ascribed to the concentration of doping ions near the grain boundaries and reduction of the grain-boundary mobility. This mechanism for reducing grain-boundary mobility has been studied theoretically as it applies to the recrystallization of metals [22,23]. Therefore, this inhibition of grain growth of the ceramics may be mainly attributed to the grain boundary aliquation [24,25]. Similar phenomenon of the suppression of grain growth induced by donor doping has been frequently observed in the ceramics such as La-modified $K_{0.5}Na_{0.5}NbO_3$ [26] and PZT [27], Nb-modified $Pb(Ti,Zr)O_3$ [22] and $BaTiO_3$–$Bi(Mg_{1/2}Ti_{1/2})O_3$–$BiFeO_3$ ceramics [24]. For the present ceramics, uniform grains and clearly demarcated grain boundaries are observed for bulk components as shown in figure 2a–g. However, the ceramics with $x = 0.0175$ and 0.02 sintered at 960°C melt down with ambiguous grain boundaries due to the over high sintering temperature for the two components.

Figure 3a shows the leakage current density J of the $Bi_{0.7}Ba_{0.3}(Fe_{0.7}Ti_{0.3})_{1-x}Nb_{0.66x}O_3$ ceramics at room temperature as a function of the electric field E; while figure 3b gives the dependences of the resistivity R of the $Bi_{0.7}Ba_{0.3}(Fe_{0.7}Ti_{0.3})_{1-x}Nb_{0.66x}O_3$ ceramics on the electric field E. As

a comparison, the J and R of pure $BiFeO_3$ prepared by an ordinary oxide sintering technique (sintered at 775°C for 2 h) are also shown in figure 3. From figure 3a and b, all the ceramics with $x = 0$–0.02 exhibit the low J values of 10^{-5}–10^{-4} A cm^{-2} and high R values of 10^9–10^{10} Ω·cm, suggesting that the $Bi_{0.7}Ba_{0.3}(Fe_{0.7}Ti_{0.3})_{1-x}Nb_{0.66x}O_3$ ceramics with $x = 0$–0.02 possess much better electric insulation than pure $BiFeO_3$ ceramics ($J = 8.18\times10^{-4}$ A cm^{-2}, $R = 2.62 \times 10^7$ Ω·cm). As well known, the poor electric insulation of pure $BiFeO_3$ is due to the valence transformation of Fe ions from Fe^{3+} to Fe^{2+} and the creation of oxygen vacancies for charge compensation during sintering [28]. The improvement in the electric insulation of the present ceramics may be ascribed to partial substitutions of Mn^{4+} and/or Ti^{4+} for Fe^{3+} in the ceramics which could suppress the formation of $Fe^{2+}_{Fe^{3+}}$ and $V_{\ddot{O}}$ [29,30]. As a result, the high resistivity of the ceramics sintered at 960°C for 2 h is obtained.

Figure 4a shows the polarization–electric field ($P-E$) hysteresis loops of the $Bi_{0.7}Ba_{0.3}(Fe_{0.7}Ti_{0.3})_{1-x}Nb_{0.66x}O_3$ ceramics measured at 6.0 kV mm^{-1}, while figure 4b shows the variations of the remanent polarization P_r and coercive field E_c with x. The saturated ferroelectric hysteresis loops were observed at $x = 0$. However, as the Nb content increases, the loops become narrower, indicating the degradation of ferroelectric activity. From figure 4b, the values of the remanent polarization P_r and coercive field E_c are 19.68 μC cm^{-2} and 3.73 kV mm^{-1}, respectively. However, P_r decreases from 6.38 to 3.11 μC cm^{-2} and E_c decreases from 4.53 to 2.41 kV mm^{-1} as x increases from 0.0025 to 0.02. Similar results about Nb-doping (Bi, Na)TiO_3–$BaTiO_3$ ceramics have been reported [31]. This is clearly different from the effect of donor ions on the ferroelectricity of Pb-based perovskite ceramics.

Figure 5 shows the variation of piezoelectric constant d_{33}, planar electromechanical coupling factor k_p, relative dielectric constant ε_r and loss tangent tan δ with x for the $Bi_{0.7}Ba_{0.3}(Fe_{0.7}Ti_{0.3})_{1-x}Nb_{0.66x}O_3$ ceramics. Similar piezoelectric properties were observed in Nb-doped PZT systems [32,33]. From figure 5a, it can be noted that the observed d_{33} decreases significantly from 133 to 19 pC N^{-1} and k_p decreases from 0.29 to 0.14 as x increases from 0 to 0.02, respectively. In general, Nb^{5+} plays a role as a donor to reduce the concentration of oxygen vacancies which was considered to be the origin of domain wall clamping, leading to an improvement in piezoelectricity and ferroelectricity of perovskite piezoelectric ceramics. However, after the addition of Nb, the present ceramics exhibit degradation in piezoelectricity and ferroelectricity. Further studies are needed to clarify the reason for the decrease in the d_{33} of $Bi_{0.7}Ba_{0.3}(Fe_{0.7}Ti_{0.3})_{1-x}Nb_{0.66x}O_3$ ceramics, especially, the effect of oxygen vacancies and crystal structure on electrical properties of the ceramics. While the observed ε_r and tan δ exhibit no obvious dependence on x as shown in figure 5b. From figure 5b, the observed dielectric constant increases significantly from 556 to 615 as x increases from 0 to 0.0025 and then increases slightly from 615 to 647 with $x = 0.0025$–0.0175. Finally, the observed dielectric constant decreases significantly to 569 as x further increases to 0.02.

It is known that the donor doping is the most important method for improving the piezoelectricity of the lead-based piezoelectric ceramics. Table 2 shows the dielectric, piezoelectric and ferroelectric properties of some donor-doped ceramics. Obviously, after donor doping, the d_{33} of the lead-based ceramics (PZT, PSZT, PZN–PZT, etc.) [16–18,34] was improved significantly. However, the lead-free

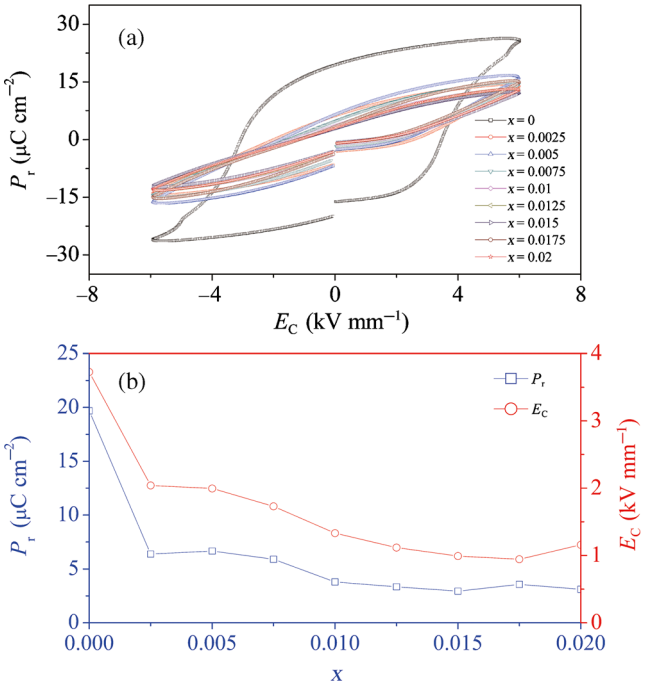

Figure 4. P–E hysteresis loops of the $Bi_{0.7}Ba_{0.3}(Fe_{0.7}Ti_{0.3})_{1-x}Nb_{0.66x}O_3$ ceramics with different x.

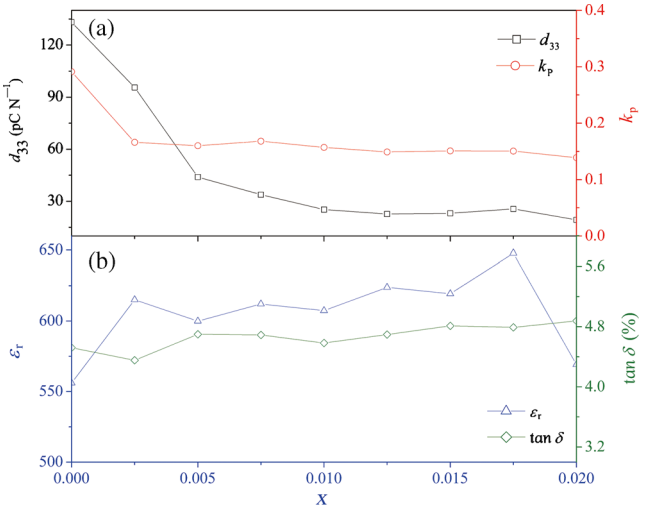

Figure 5. (**a**) Variations of piezoelectric coefficient d_{33} and electromechanical coupling factors k_p for the $Bi_{0.7}Ba_{0.3}(Fe_{0.7}Ti_{0.3})_{1-x}Nb_{0.66x}O_3$ ceramics and (**b**) variations of the dielectric constant ε_r and the loss tangent tan δ with x for the $Bi_{0.7}Ba_{0.3}(Fe_{0.7}Ti_{0.3})_{1-x}Nb_{0.66x}O_3$ ceramics.

Table 2. Dielectric, piezoelectric and ferroelectric properties of the donor-doped ceramics.

Materials	d_{33} (pC N^{-1})	k_p (%)	ε_r	tan δ (%)	T_C (°C)	P_r (μC cm^{-2})	E_c (kV mm^{-1})
BFO–BT	116.4	0.27	650	4.81	578	18	2.28
0.25% mol Nb–BFO–BT	95.6	0.17	615	4.35	614	7	2.04
PSZT [34]	305	0.44	—	0.44	—	—	—
1% mol La–PSZT [16]	640	0.56	—	1.55	—	—	—
0.3PZN–0.7PZT + 0.3wt% Li_2CO_3 [16]	398	0.63	1942	0.02	410	—	—
0.3%Sm_2O_3–0.3PZN–0.7PZT + 0.3wt% Li_2CO_3 [16]	483	0.65	2525	0.02	394	—	—
PZT [17]	~240	—	~1050	—	—	—	—
Nb-PZT [18]	~385	~0.62	1225	0.02	—	—	—
KNN [19]	86	—	352	0.13	—	13.8	1.73
0.5% mol Ba and Ca–KNN [19]	90(105)	—	366(293)	0.08(0.06)	—	14.3(16)	1.28(1.24)

BFO: $BiFeO_3$; BT: $BaTiO_3$; PSZT: $Pb_{0.95}Sr_{0.05}(Zr_{0.54}Ti_{0.46})O_3$; PZN–PZT: $Pb(Zn_{1/3}Nb_{2/3})O_3$–$PbZr_{0.49}Ti_{0.51}O_3$; PZT: $Pb(Zr_{0.92}Ti_{0.08})O_3$, $Pb(Zr_{0.52}Ti_{0.48})O_3$; KNN: $K_{1/2}Na_{1/2}NbO_3$.

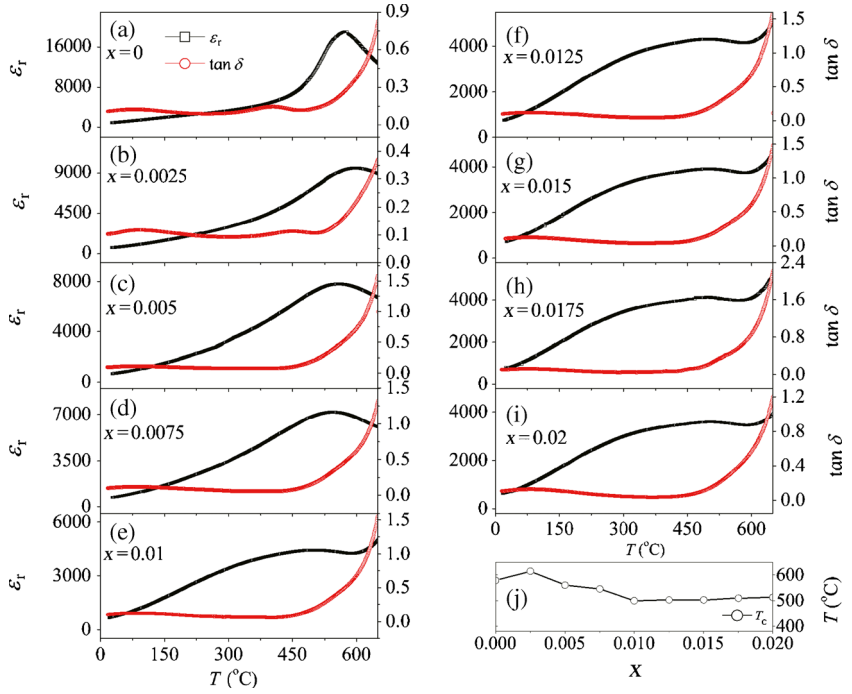

Figure 6. (**a–i**) Temperature dependences of relative dielectric constant ε_r and loss tangent tan δ at 1 MHz for the $Bi_{0.7}Ba_{0.3}(Fe_{0.7}Ti_{0.3})_{1-x}Nb_{0.66x}O_3$ ceramics sintered at 960°C for 2 h and (**j**) variations in T_C of the $Bi_{0.7}Ba_{0.3}(Fe_{0.7}Ti_{0.3})_{1-x}Nb_{0.66x}O_3$ ceramics.

(KNN) ceramic [19] exhibit very slight enhancement after the donor doping. This result indicate that the donor doping for lead-based and lead-free ceramics exhibit different doping effects, which should be studied further. For present ceramics sintered at 960°C for 2 h, the Nb doping leads to lower piezoelectric and weaker ferroelectric properties. This result may be ascribed to the decreases in grain size. As is well known, the ferroelectricity has an approximately positive relationship with the grain size and the correlation of domain size and grain size can be defined as (domain size) $\propto$ (grain size)^m (m is related to the grain size) [35,36]. Therefore, the domain boundary increases as grain size and domain size decrease and thus weaker polarization is obtained in the ceramics with small grains than in those with large grains [37].

Figure 6a–i shows temperature dependences of relative dielectric constant ε_r and loss tangent tan δ at 1 MHz for the $Bi_{0.7}Ba_{0.3}(Fe_{0.7}Ti_{0.3})_{1-x}Nb_{0.66x}O_3$ ceramics, while the variation in Curie temperature T_C of the $Bi_{0.7}Ba_{0.3}(Fe_{0.7}Ti_{0.3})_{1-x}Nb_{0.66x}O_3$ ceramics are shown in figure 6j. All the ceramics exhibit a dielectric peak at T_C. From figure 6a–i, the $Bi_{0.7}Ba_{0.3}(Fe_{0.7}Ti_{0.3})_{1-x}Nb_{0.66x}O_3$ ceramic with $x = 0$ exhibit a sharp dielectric peak related to the normal ferroelectric to paraelectric transition at T_C. However, the dielectric peaks become boarder after the addition of Nb, indicating that a diffuse phase transition is induced in the ceramics with

high Nb level, which may attribute to the cation disorder and the compositional fluctuate of the ceramics caused by Nb doping [38]. From figure 6j, the observed T_C increases from 578 to 603°C with x increasing from 0 to 0.0025 and then decreases greatly to 503°C with x increasing to 0.015, finally increases slightly from 509 to 513°C with x further increasing from 0.0175 to 0.02. Obviously, a small amount of Nb doping ($x = 0.0025$) can improve the T_C of the ceramics.

4. Conclusions

Lead-free $Bi_{0.7}Ba_{0.3}(Fe_{0.7}Ti_{0.3})_{1-x}Nb_{0.66x}O_3$+1 mol% MnO_2 ceramics with $x = 0$, 0.0025, 0.05, 0.075, 0.01, 0.0125, 0.015, 0.0175 and 0.02 were synthesized by conventional solid-state reaction method and the effect of the Nb doping on microstructure, ferroelectric and piezoelectric properties of the ceramics were studied. The grain growth of the ceramics is inhibited after the addition of Nb doping. High electric insulation ($R = 10^9$–10^{10} Ω·cm) and the poor piezoelectric performance and weak ferroelectricity are observed with Nb_2O_5 addition in the ceramics. The $Bi_{0.7}Ba_{0.3}(Fe_{0.7}Ti_{0.3})_{1-x}Nb_{0.66x}O_3 + 1$ mol% MnO_2 ceramic with $x = 0$ exhibits the optimum piezoelectric properties with $d_{33} = 133$ pN C^{-1} and $k_p = 0.29$ and high Curie temperature ($T_C = 603$°C).

Acknowledgements

This work was supported by the projects of Education Department of Sichuan Province (11ZA104), Science and Technology Bureau of Sichuan Province (2010JQ0046) and the Open Project of State Key Laboratory of Electronic Thin Films and Integrated Devices of University of Electronic Science and Technology of China (KFJJ201108).

References

[1] Qin H B, Zhang H L, Zhang B P and Xu L H 2011 *J. Am. Ceram. Soc.* **94** 3671
[2] Prasatkhetragarn A, Muangkonkad P, Aommongkol P, Jantaratana P, Vittayakorn N and Yimnirun R 2013 *Ceram. Int.* **39** S249
[3] Wang Q Q, Wang Z, Liu X Q and Chen X M 2012 *J. Am. Ceram. Soc.* **95** 670
[4] Patil D R, Lokare S A, Devan R S, Chougule S S, Kolekar Y D and Chougule B K 2007 *J. Phys. Chem. Solids* **68** 1522
[5] Varshney D, Kumar A and Verma K 2011 *J. Alloys Compd.* **509** 8421
[6] Azough F, Freer R, Thrall M, Cernik R, Tuna F and Collison D 2010 *J. Eur. Ceram. Soc.* **30** 727
[7] Zhang Q, Zhu X H, Xu Y H, Gao H B, Xiao Y J, Liang D Y *et al* 2013 *J. Alloys Compd.* **546** 57
[8] Basu S, Hossain S K M, Chakravorty D and Pal M 2011 Curr. Appl. Phys. **11** 976
[9] Jianguo Zhao, Xianghui Zhang, Shijiang Liu, Weiying Zhang and Zhaojun Liu 2013 *J. Alloys Compd.* **557** 120
[10] Matsuo H, Noguchi Y, Miyayama M, Suzuki M and Watanabe A 2010 *J. Appl. Phys.* **108** 104103
[11] Liu X H, Xu Z, Wei X Y, Dai Z H and Yao X 2010 *J. Am. Ceram. Soc.* **93** 2975
[12] Pandey D and Singh A 2009 *Bull. Mater. Sci.* **32** 361
[13] Wei Y X, Wang X T, Zhu J T, Wang X L and Jia J J 2013 *J. Am. Ceram. Soc.* **96** 3163
[14] Leontsev S O and Eitel R E 2009 *J. Am. Ceram. Soc.* **92** 2957
[15] Yang H B, Zhou C R, Liu X Y, Zhou Q, Chen G H, Li W Z and Wang H 2013 *J. Am. Ceram. Soc.* **33** 1177
[16] Fan G F, Shi M B, Lu W Z, Wang Y Q and Liang F 2014 *J. Eur. Ceram. Soc.* **34** 23
[17] Chen B H, Huang C L and Wu L 2004 *Solid-State Electron.* **48** 2293
[18] Zhuang Z Q, Haun M J, Jang S J and Cross L E 1989 *IEEE Trans. Ultrason. Ferroelectr. Freq. Control* **36** 413
[19] Taub J, Ramajo L and Castro M S 2013 *Ceram. Int.* **39** 3555
[20] Lutterotti L 2011 MAUD—material analysis using diffraction, http://www.ing.unitn.it/~maud/index.html
[21] Yang H B, Zhou C R, Liu X Y, Zhou Q, Chen G H, Wang H and Li W Z 2012 *Mater. Res. Bull.* **47** 4233
[22] Pereira M, Peixoto A G and Gomes M J M 2001 *J. Eur. Ceram. Soc.* **21** 1353
[23] Atkin R B and Fulrath R M 1971 *J. Am. Ceram. Soc.* **54** 265
[24] Yabuta H, Shimada M, Watanabe T, Hayashi J, Kubota M, Miura K *et al* 2012 *Jpn. J. Appl. Phys.* **51** 09LD04
[25] Yi J Y, Lee J K and Hong K S 2004 *Jpn. J. Appl. Phys.* **43** 6188
[26] Gao D J, Kwok K W, Lin D M and Chan H L W 2009 *J. Phys. Appl. Phys.* **42** 035411
[27] Pdungsap L, Udomkan N, Boonyuen S and Winotaia P 2005 *Sens. Actuat. A* **122** 250
[28] Wu J G, Kang G Q and Wang J 2009 *Appl. Phys. Lett.* **95** 192901
[29] Chauhana S, Kumara M, Chhokera S, Katyal S C, Singh H, Jewariya M and Yadav K L 2012 *Solid State Commun.* **152** 525
[30] Lin D, Zheng Q J, Li Y, Wan Y and Zhou Q L W 2013 *J. Eur. Ceram. Soc.* **33** 3023
[31] Chen L, Luo B C, Chan N Y, Dai J Y, Hoffman M, Li S and Wang D Y 2014 *J. Alloys Compd.* **587** 339
[32] Kayasu V and Ozenbas M 2009 *J. Eur. Ceram. Soc.* **29** 1157
[33] Tanasoiu C, Dimitriu E and Miclea C 1999 *J. Eur. Ceram. Soc.* **19** 1187
[34] Kalem V, Cam I and Timucin M 2011 *Ceram. Int.* **37** 1265
[35] Randall C A, Kim N, Kucera J P, Cao W and Shrout T R 1998 *J. Am. Ceram. Soc.* **81** 677
[36] Cao W and Randall C A 1996 *J. Phys. Chem. Solids* **57** 1499
[37] Yan Y, Cho K H and Priya S 2011 *J. Am. Ceram. Soc.* **94** 3953
[38] Petnoi N, Bomlai P, Jiansirisomboon S and Watcharapasorn A 2013 *Ceram. Int.* **39** S113